Sensor and Simulation Notes

Note 524

October 2007

Experimental Setups For Two-Arm and 60^o Four-Arm Prolate-Spheroidal Impulse-Radiating Antenna (IRA)

Serhat Altunc, Carl E. Baum, Christos G. Christodoulou, Edl Schamiloglu and Jerald Buchenauer

University of New Mexico
Department of Electrical and Computer Engineering
Albuquerque New Mexico 87131

Abstract

Experimental setups using two-arm and 60^o four-arm prolate-spheroidal IRAs are used to obtain better focusing for a prolate-spheroidal IRA and these results are compared with analytical results in [1] for comparison. This paper presents a summary of the experimental setup and the dimensions of these experiments are based on [1, 2]. These setups were motivated by a biological application [3].

This work was sponsored in part by the Air Force Office of Scientific Research.

1 Introduction

Experiments for two-arm and 60^o four-arm prolate-spheroidal IRAs are used to obtain better focusing for a prolate-spheroidal IRA. They were performed at the University of New Mexico (UNM) Transient Antenna Laboratory in order to compare our experimental results with our analytical and numerical results.

We feed our IRA using a $V_0 = 0.5\,V$ (peak-peak 1 V) and $t_\delta = 100\,ps$, rise time ramp-rising step. The analytical focal waveforms are presented in Figure 1 for this excitation.

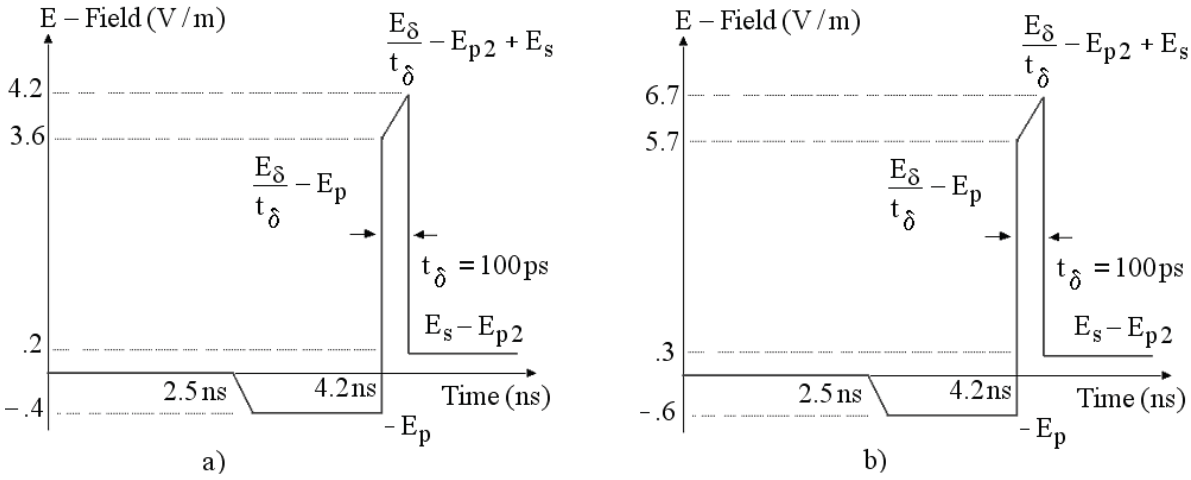

Figure 1: Analytical focal waveforms a) two-arms b) 60^o four-arms.

We use maximum t_{mr} (based on maximum rate of rise) as t_δ to compare our experimental results with analytical results.

For a step-like $f(t)$, the t_{mr} is

$$t_{mr} = \frac{f_{max}}{\left.\frac{df}{dt}\right|_{max}}. \qquad (1.1)$$

2 Experimental Setup and Data Analysis Technique

The experimental setup basically includes three components. These are a prolate-spheroidal reflector with feed arms, a sampling-oscilloscope, and a pulse generator. They are presented in Figures 2 and 6.3.

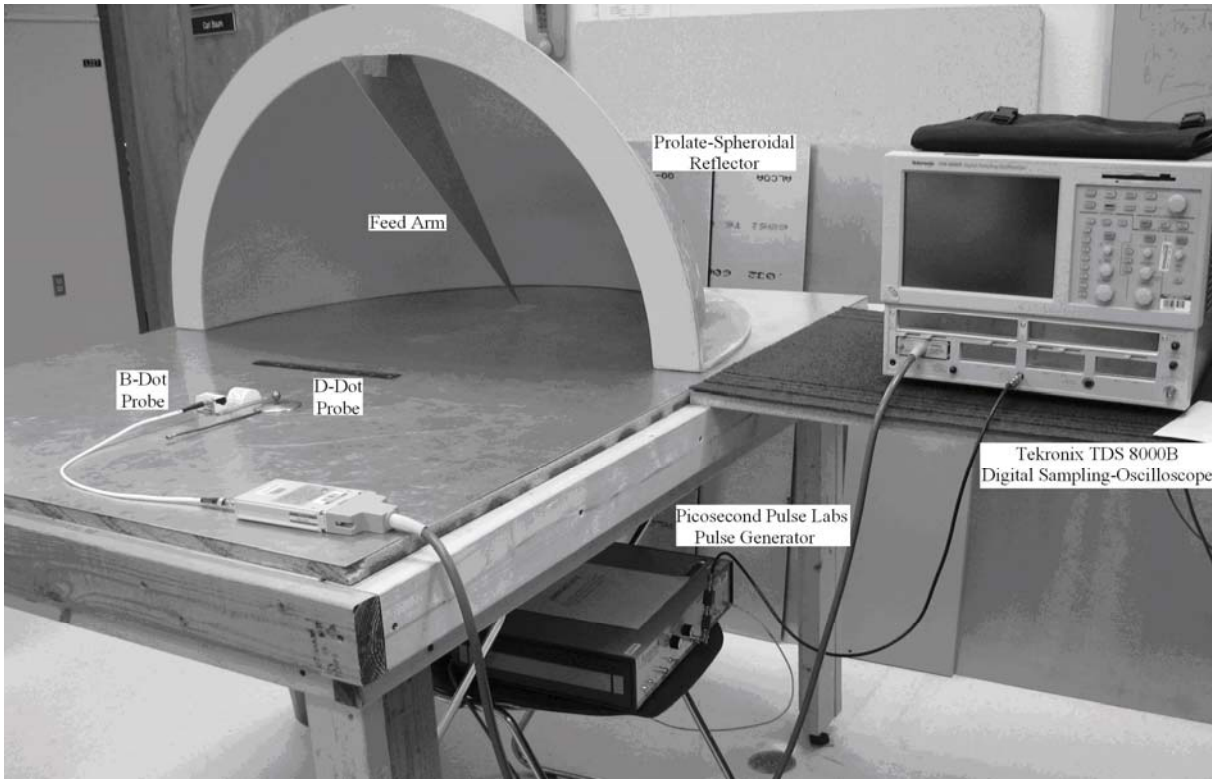

Figure 2: Experimental setup for a two-feed arm prolate-spheroidal IRA.

Figure 3: Experimental setup for a 60^{O} four-feed arm prolate-spheroidal IRA.

As seen from Figure 4, we use a Tektronix TDS 8000B Digital Sampling-Oscilloscope to measure the waveform at the second focal point. A Picosecond Pulse Labs pulser with a PSPL 4050 RPH fast pulser head generator is used for excitation. The output of the step generator is a 45-ps rise time, 10 V amplitude. We have also used a 10 dB attenuator to decrease the voltage level for safety reasons. Two nano second and three nano second long cables are used to connect the pulser to the feed arms and sensors to the sampling oscilloscope.

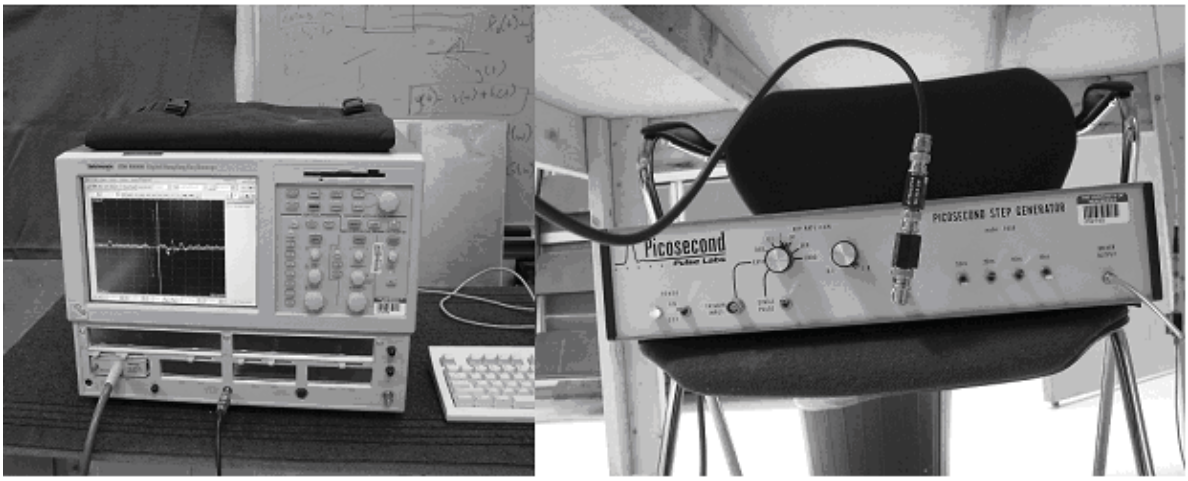

Figure 4: Sampling-oscilloscope and pulse generator.

The feed arms' dimensions are calculated in Chapter 4 (Table 4.1 and 4.2) and they are presented in Figure 5. The feed arms are 0.8 cm thick.

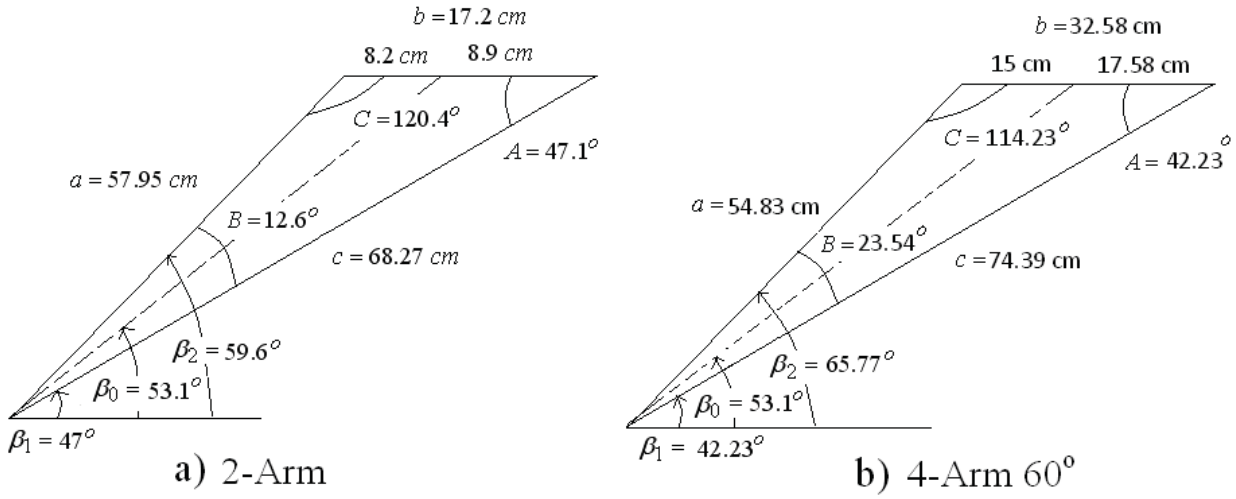

Figure 5: Two-feed arms and 60^{o} four-feed arms dimensions and angles.

One can see the 60^{o} four-feed arms IRA in Figure 6 and how it is inserted in the reflector. We use foam with a relative dielectric constant $\varepsilon_r = 1.013$ to maintain the feed arms angle at 60^{o}.

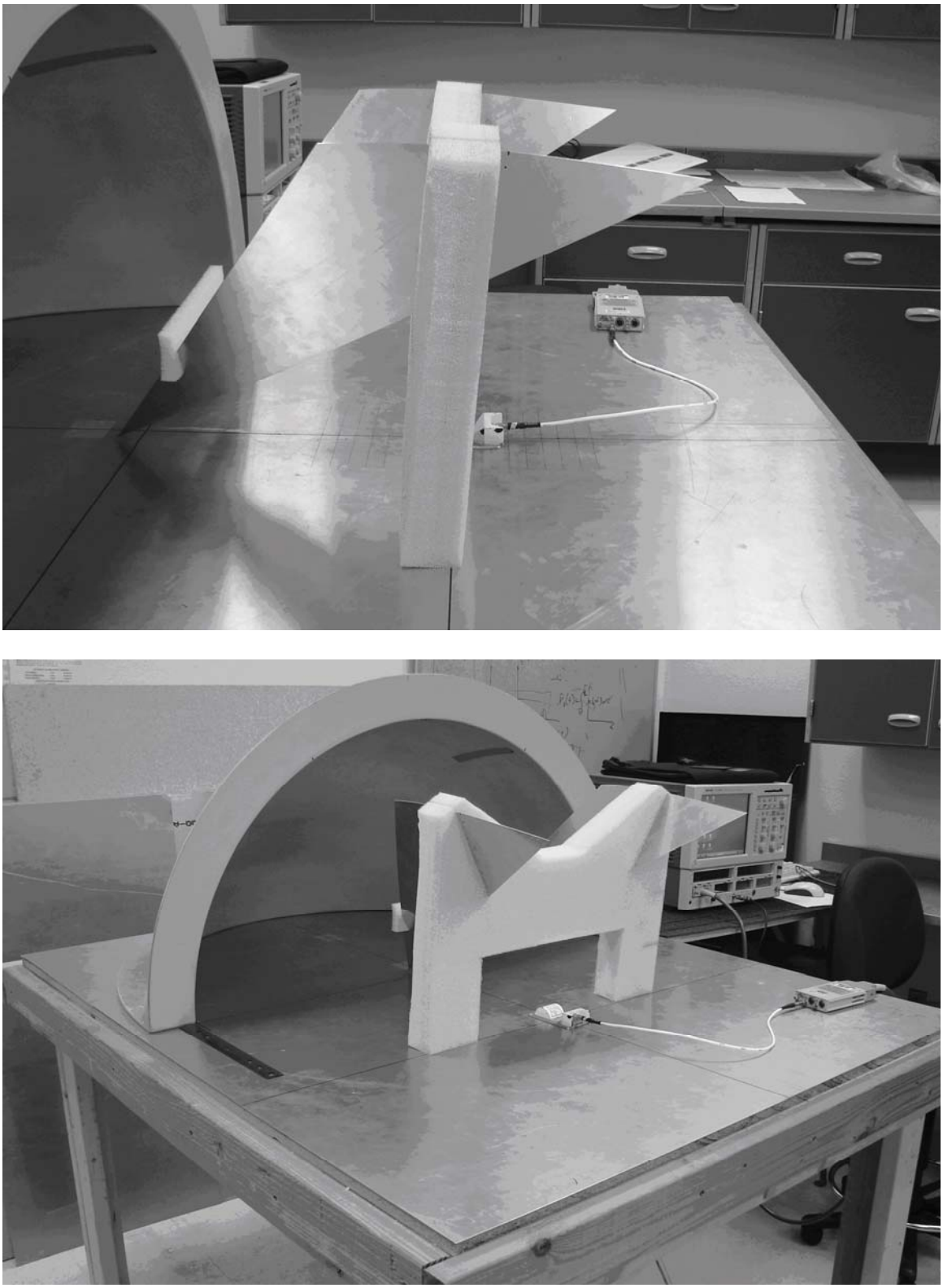

Figure 6: 60^{o} four-feed arms used in one of the IRAs.

Fast D-Dot, slow D-Dot and B-Dot probes are used for field measurements and are presented in Figure 7. We use the B-Dot probe to obtain the magnetic field and also use the prepulse data of the B-Dot probe to calibrate the slow D-Dot probe data. We use the data from the B-dot probe which has an equivalent area $A_{eq} = 1\ cm^2$ and analyze the data as follows:

$$V = A_{eq}\frac{dB}{dt}, \text{ and}$$
$$B = \frac{1}{A_{eq}}\int_{-\infty}^{t} V(t')\,dt'. \qquad (2.1)$$

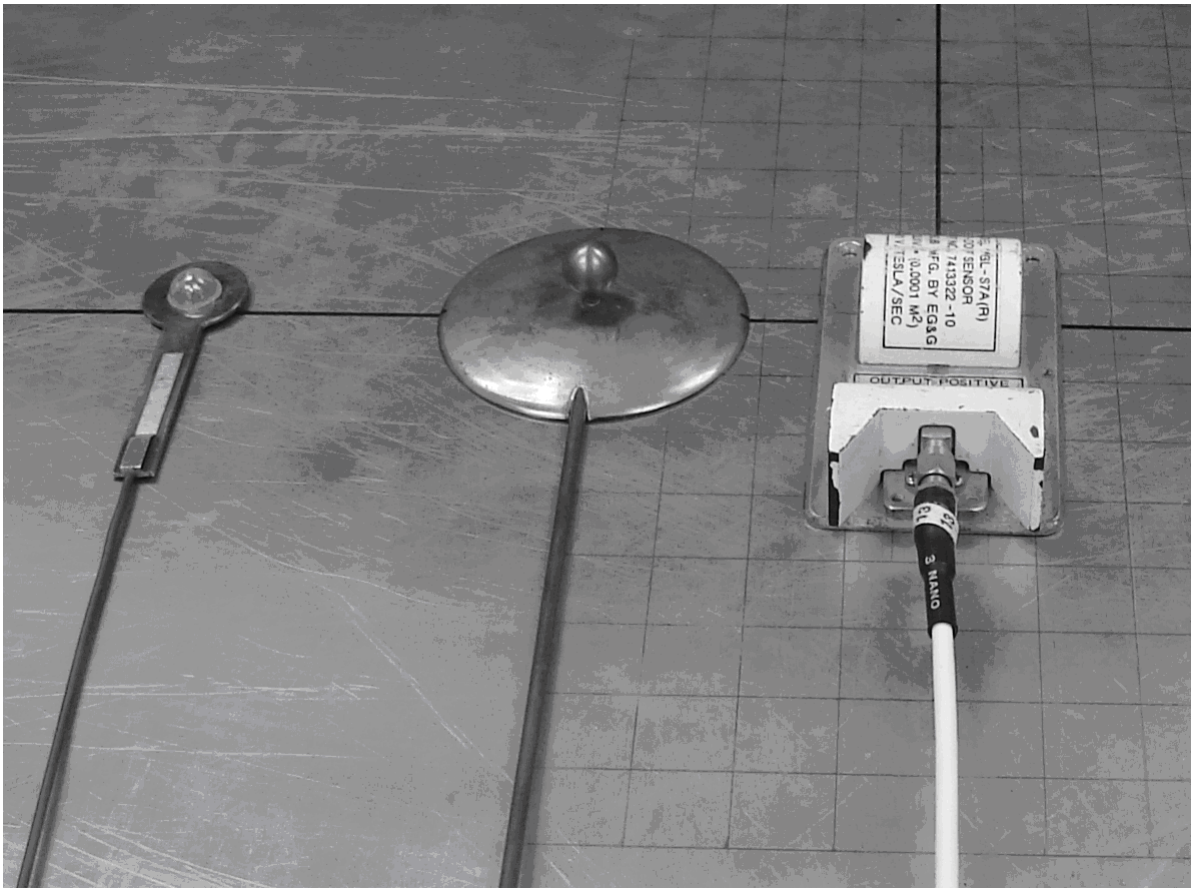

Figure 7: Fast D-Dot, slow D-Dot and B-Dot probes (from left to right) used for measurements.

We can find the equivalent electric field as

$$E_{eq} = cB = \frac{c}{A_{eq}} \int_{-\infty}^{t} V(t')\,dt' . \tag{2.2}$$

This equivalent electric field, E_{eq}, gives the exact result for the prepulse because we have a TEM wave and $E/H = \eta_0 \approx 377\,\Omega$ for free space. We calibrate our D-Dot data by comparing the prepulse term. We obtain the data from the D-Dot probe and analyze it as follows:

$$\begin{aligned} I &= \frac{V}{Z_0} = A_{eq}\frac{dD}{dt}, \text{ and} \\ E &= \frac{1}{\varepsilon_0 Z_0 A_{eq}} \int_{-\infty}^{t} V(t')\,dt' . \end{aligned} \tag{2.3}$$

Our pulse generator has a $V_0 = 10\,V$ excitation. We feed our IRA with

$$V = T\,V_0 , \tag{2.4}$$

where T is the transmission coefficient

$$T = \frac{2Z_L}{Z_L + Z_0} . \tag{2.5}$$

The pulse impedances for the two-arm and 60^o four-feed arm cases are $400\,\Omega$ and $200\,\Omega$, respectively. Since we are using a ground plane $Z_L = 200\,\Omega \; and \; 100\,\Omega$, respectively. The transmission coefficients are 1.6 and 1.33. In our analytical calculation we use $V_0 = 0.5\,V$ and then normalize the data to obtain the electric field as

$$E_N = \frac{1}{20\,T\,\varepsilon_0 Z_0 A_{eq}} \int_{-\infty}^{t} V(t')\,dt . \tag{2.6}$$

3 Experimental Results Normalized to 1 Volt Differential Input

Figures 8 and 9 shows that the results for the focal waveforms are close to each other, but for the slow D-Dot sensor we do not have much oscillation in the postpulse since it has a slower frequency response. Although we do not have TEM waves for the impulse, we calculate $\eta = E/H$. For the two-arm case η is 384, for the four-arm case

η is 408. However in free space $\eta_0 = 377\,\Omega$. This proves that we do not have a purely TEM wave for the impulse.

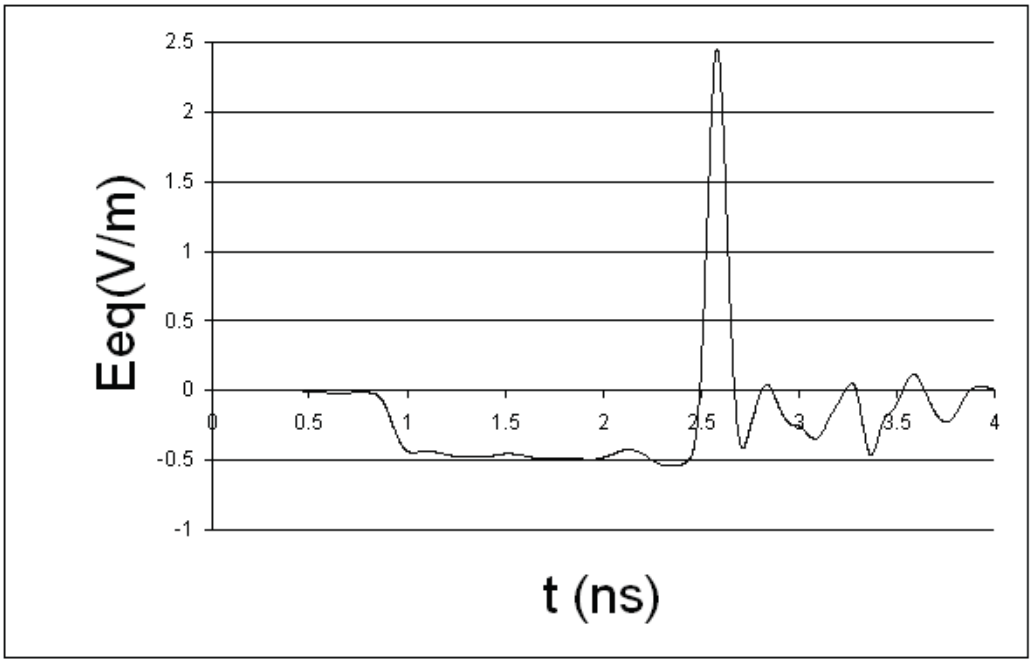

a)

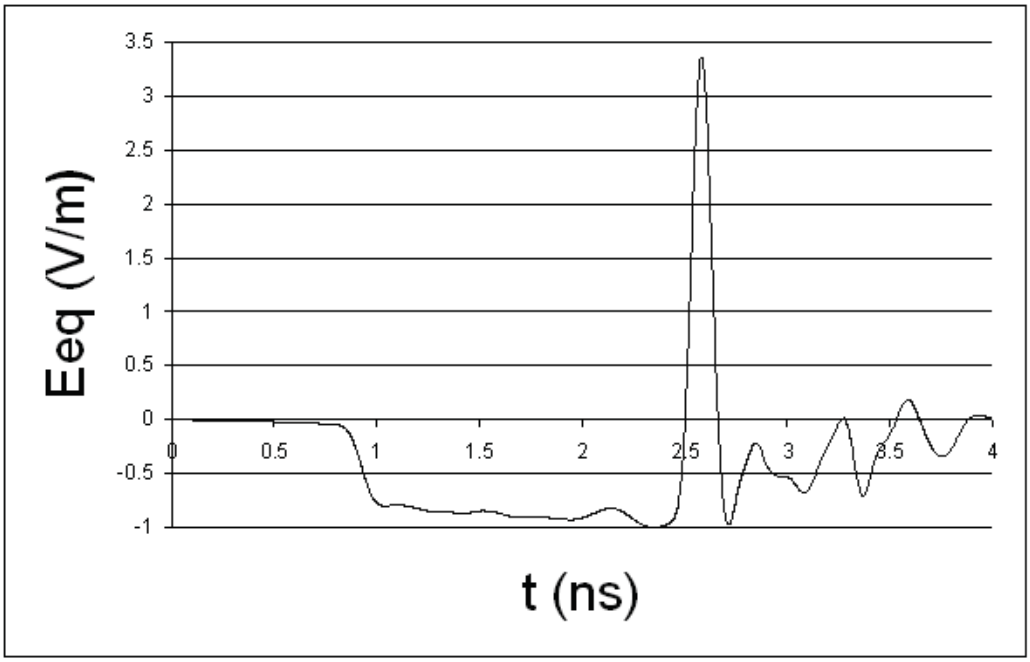

b)

Figure 8: B-Dot probe focal waveforms, E_{eq}, a) two-arms and b) 60^{o} four-feed arms.

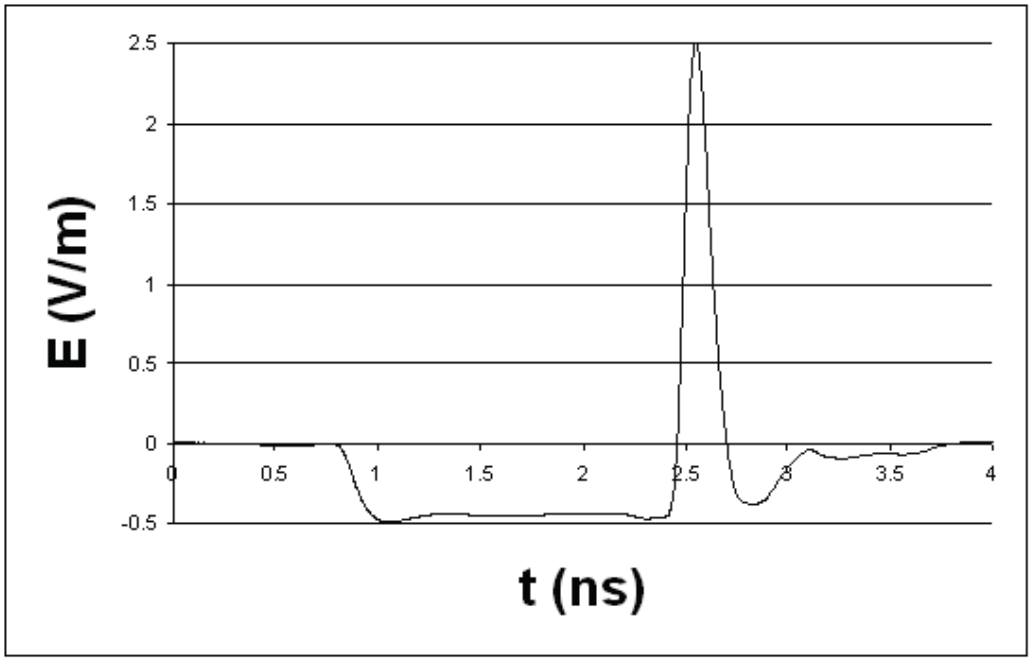

a)

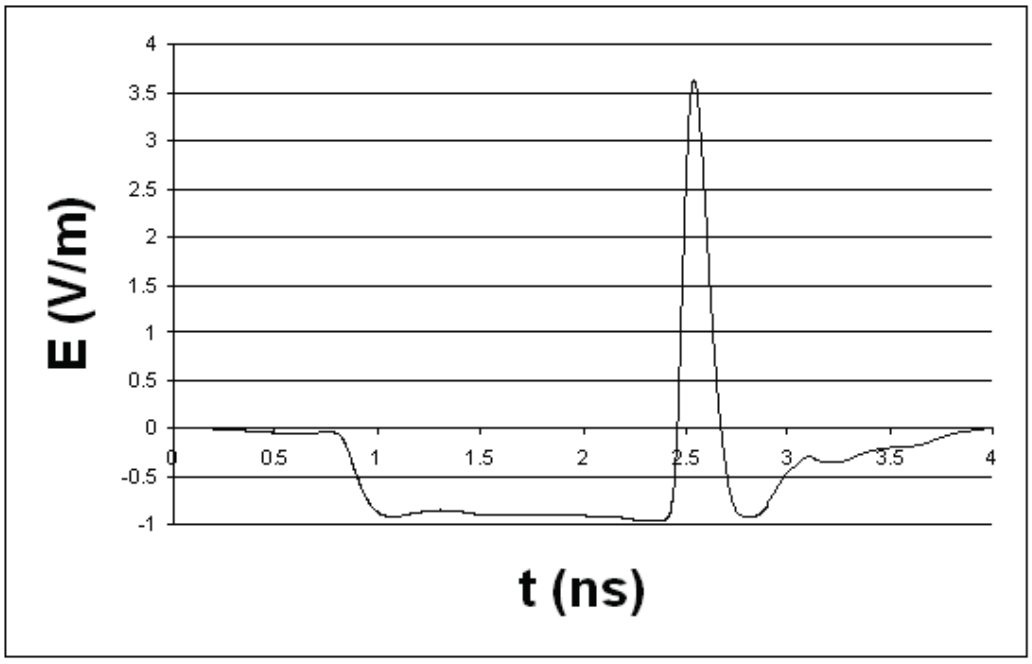

b)

Figure 9: Slow D-Dot probe focal waveforms a) two-arms and b) 60^{o} four-feed arms.

We can see from Figure 10 that if we use the fast D-Dot sensor we have this oscillation. The oscillation may not be due to the different type of sensors we are using.

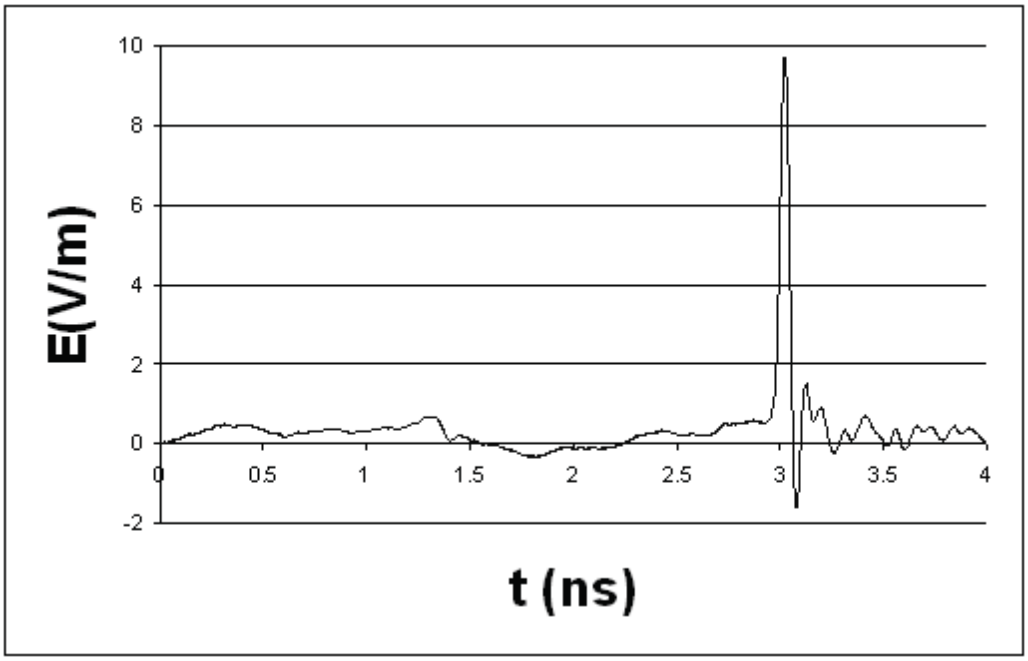

a)

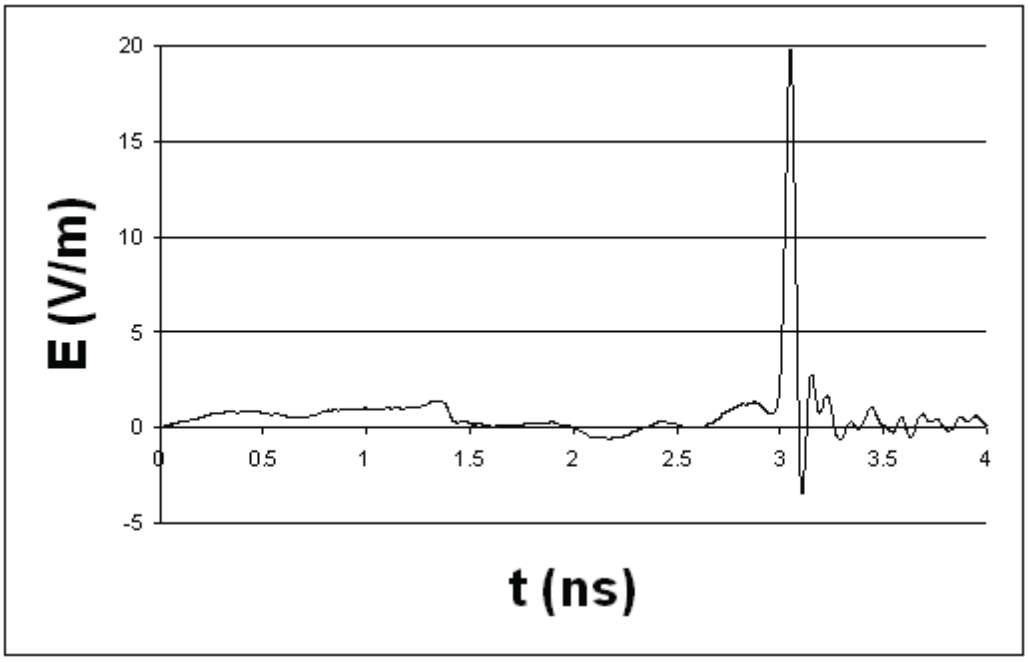

b)

Figure 10: Fast D-Dot probe focal waveforms and a) two b) 60^{o} four-feed arms.

Figure 11 presents a comparison of the focal waveform from the B-Dot and the normalized focal waveform from the fast D-dot. They oscillate at different frequencies. The fast D-Dot sensor response is very fast; this can cause differences in the postpulse. We do not have that much ringing in the slow D-Dot postpulse. The B-Dot sensor shows a 3 GHz ringing.

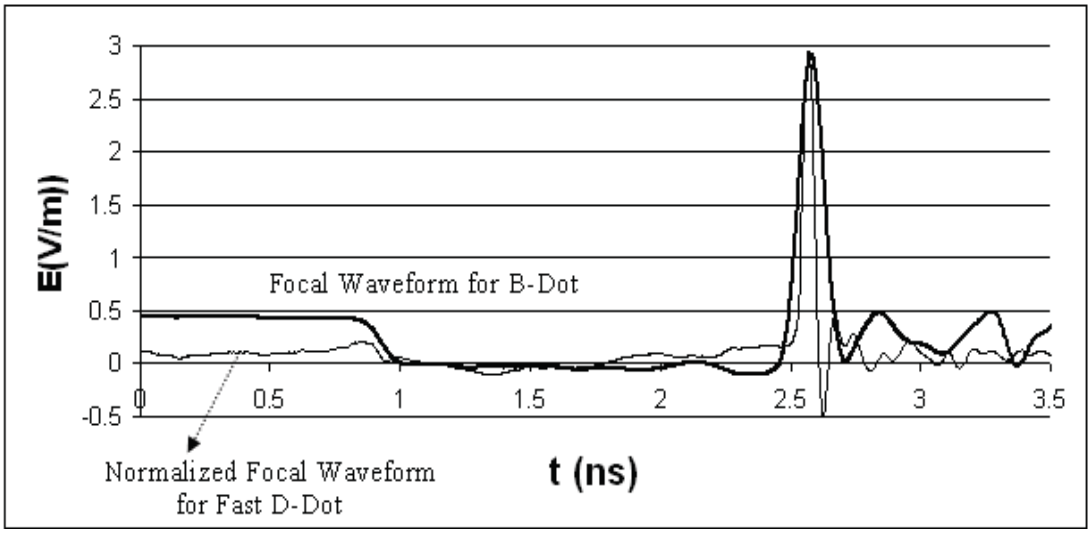

Figure 11: Focal waveform from the B-Dot and normalized focal waveform from the fast D-Dot measured of the two-arm IRA.

We connect the B-Dot probe directly to the oscilloscope. Figure 12 shows the measured reflection coefficient and arrows show the ringing that can cause the postpulse oscillations.

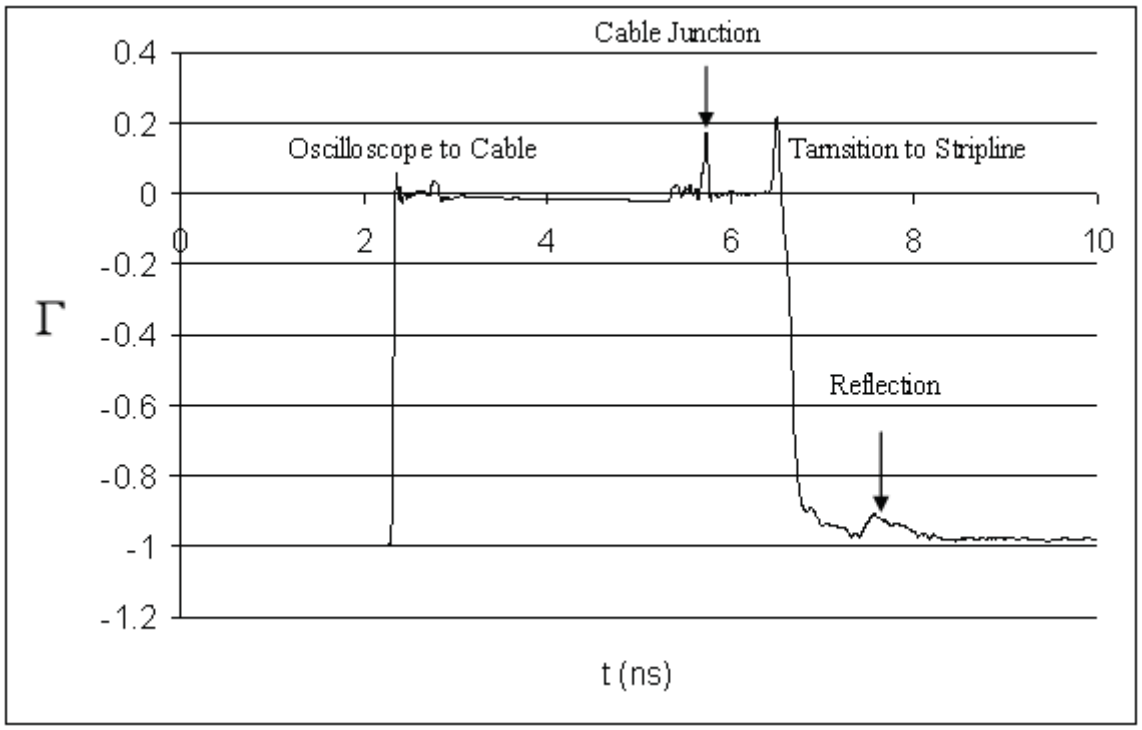

Figure 12: Reflection coefficient (Γ) measurements : The B-Dot probe directly connected to the oscilloscope.

There will always be causes for oscillations and aberrations at the levels observed in the fast D-dot trace. There are cable and connection non uniformities, nonlinear effects in the sampler, sampling time errors, digitizing errors, etc. Most importantly, the generator signal is not pure and has lots of aberrations following the step.

4 Conclusion

Table 1: Maximum values of the Eeq variation along the *y* and *z* -axis from the B-Dot sensor.

	Focal E(V/m)	y<0, z=0	E (V/m)	y>0, z=0	E (V/m)	y=0, z<0	E (V/m)	y=0, z>0	E (V/m)
2 Arm	2.45	y=-2cm	2.27	y=2cm	2.01	z=-1cm	2.46	z=1cm	2.41
		y=-4cm	2.27	y=4cm	1.44	z=-2cm	**2.47**	z=2cm	2.40
		y=-6cm	1.15	y=6cm	0.97	z=-4cm	2.35	z=4cm	2.28
		y=-8cm	0.79	y=8cm	0.66	z=-6cm	2.21	z=6cm	2.18
						z=-8cm	2.03	z=8cm	2.07
						z=-10cm	1.80	z=10cm	1.95
						z=-12cm	1.57	z=12cm	1.69
						z=-14cm	1.30	z=14cm	1.48
						z=-16cm	1.12	z=16cm	1.38
4 Arm	3.36	y=-2cm	2.95	y=2cm	2.56	z=-1cm	3.41	z=1cm	3.32
		y=-4cm	2.94	y=4cm	1.50	z=-2cm	**3.42**	z=2cm	3.27
		y=-6cm	1.02	y=6cm	0.94	z=-4cm	3.25	z=4cm	3.13
		y=-8cm	0.86	y=8cm	0.89	z=-6cm	2.90	z=6cm	3.01
						z=-8cm	2.65	z=8cm	2.85
						z=-10cm	2.35	z=10cm	2.69
						z=-12cm	2.26	z=12cm	2.35
						z=-14cm	1.85	z=14cm	2.09
						z=-16cm	1.52	z=16cm	1.93

As seen in Table 1, our focal point is about 2 cm closer to the reflector because we do not have sufficient high frequency components and we also have a step term E_s affecting of the amplitude of impulse. Figure 4.3 shows that the amplitude of the impulse is proportional to E_δ and E_s, but E_δ is the dominant term. The E_δ value is larger for high frequencies and E_s is larger at the aperture plane. E_s decreases more than E_δ toward the focal point. Thus we have two computing parameters, E_δ and E_s. Because of these two terms, our peak point is 2 cm closer to the reflector. At the focal point our prolate-spheroidal IRA works like a differentiator or high-pass filter, high frequencies contribute more than low frequencies.

Although the amplitudes of the electric fields should be symmetric along the *x*-axis with respect to x=0, they are different. We believe this is because of errors in the geometric shape or alignment of the prolate-spheroidal reflector.

The slow sensors are more sensitive than the fast D-Dot sensor, but they are not fast enough to obtain the actual t_{mr} values. We obtain larger t_{mr} values which result in a

decrease in the amplitude of the impulse part of the focal waveform. If we use the fast D-Dot sensor, it is not sensitive enough. We obtain higher amplitudes in the impulse part, whereas we obtain more differences in the amplitude of the impulse part of the focal waveform. The analytical, experimental results, oscillation amplitude, t_{mr} and differences in experimental results compared to the analytical results are summarized in Table 2.

Table 2: Analytical, experimental results, oscillation amplitude, t_{mr} and difference in experimental results compared to analytical results.

	Analytical peaks(V/m)	Exp results(V/m)	Oscillation(V/m)	tmr(ps)	Difference(%)
B-Dot 2 Arm	2.96 - 3.55	2.5	0.4	119	21.4
B-Dot 4 Arm	4.4-5.3	3.5	0.97	127	32.7
D-Dot 2 Arm slow	2.96 - 3.55	2.5	0.38	119	21.4
D-Dot 4 Arm slow	4.3-5.2	3.5	0.92	130	32.7
D-Dot 2 Arm fast	14.7-15.3	9.6	1.58	26.5	36.0
D-Dot 4 Arm fast	28.4-29.4	19.8	3.3	22	31.5

There are several factors that can lead to differences in the analytical expressions and experiments. When the focal fields are calculated in Chapter 4 and [3], the aperture integral did not consider the feed arms and feed-arms' thicknesses. This can cause an error in the calculation of the impulse amplitude of the focal waveform.

There are errors in the experiments that need to be accounted for. We are in the limit of our instrumentation, we have less accuracy because of the limitation of the probes.

We have checked the pulser and the connection cables to find the reason for the postpulse oscillations. These results are presented in Figure 13. One can see from Figure 13 that the postpulse oscillations are not related to the pulser or the 2 nano-second and 3 nano-second long cables that we use to connect the pulser to the feed arms and sensors to the sampling oscilloscope. They are not oscillating at the same frequencies and they do not have the same amplitudes. We do not have any problem with the pulser and connection cables.

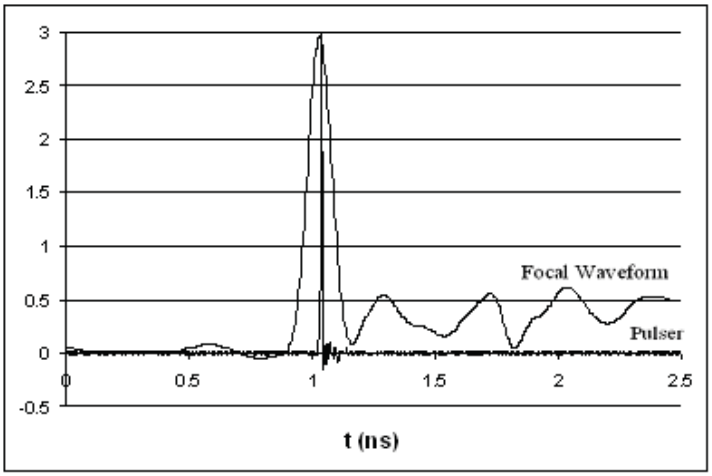

a)

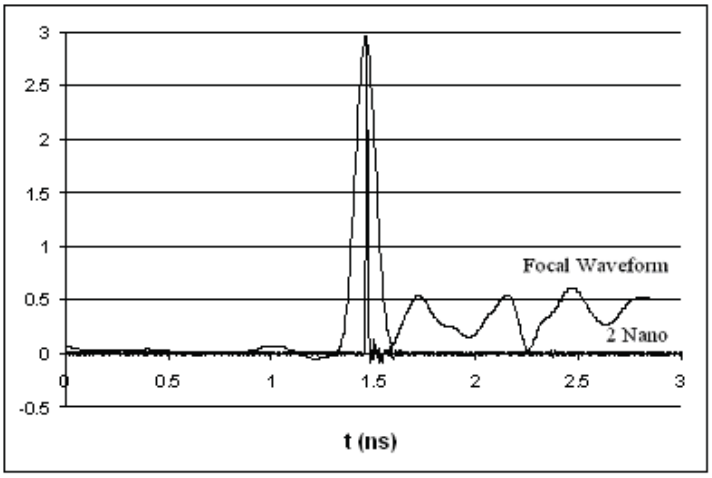

b)

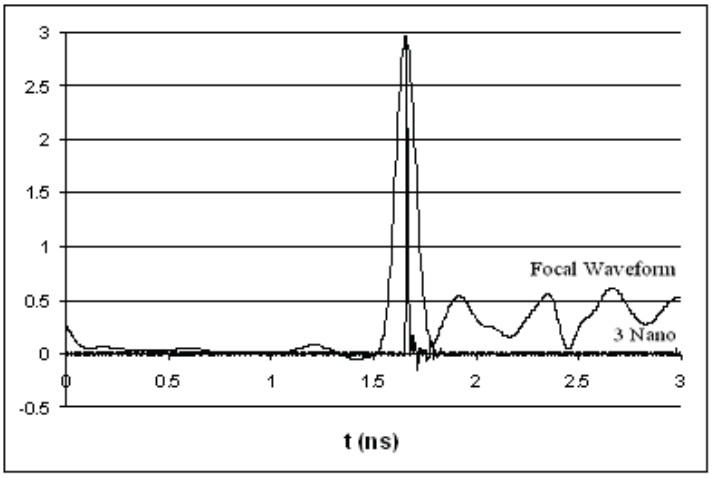

c)

Figure 13: The focal waveform from the B-Dot sensor: a) the normalized data from the pulser, b) with 2 nano-second, c) with 3 nano-second long cable.

We next checked the prepulse term and took its derivative, shown in Figure 14

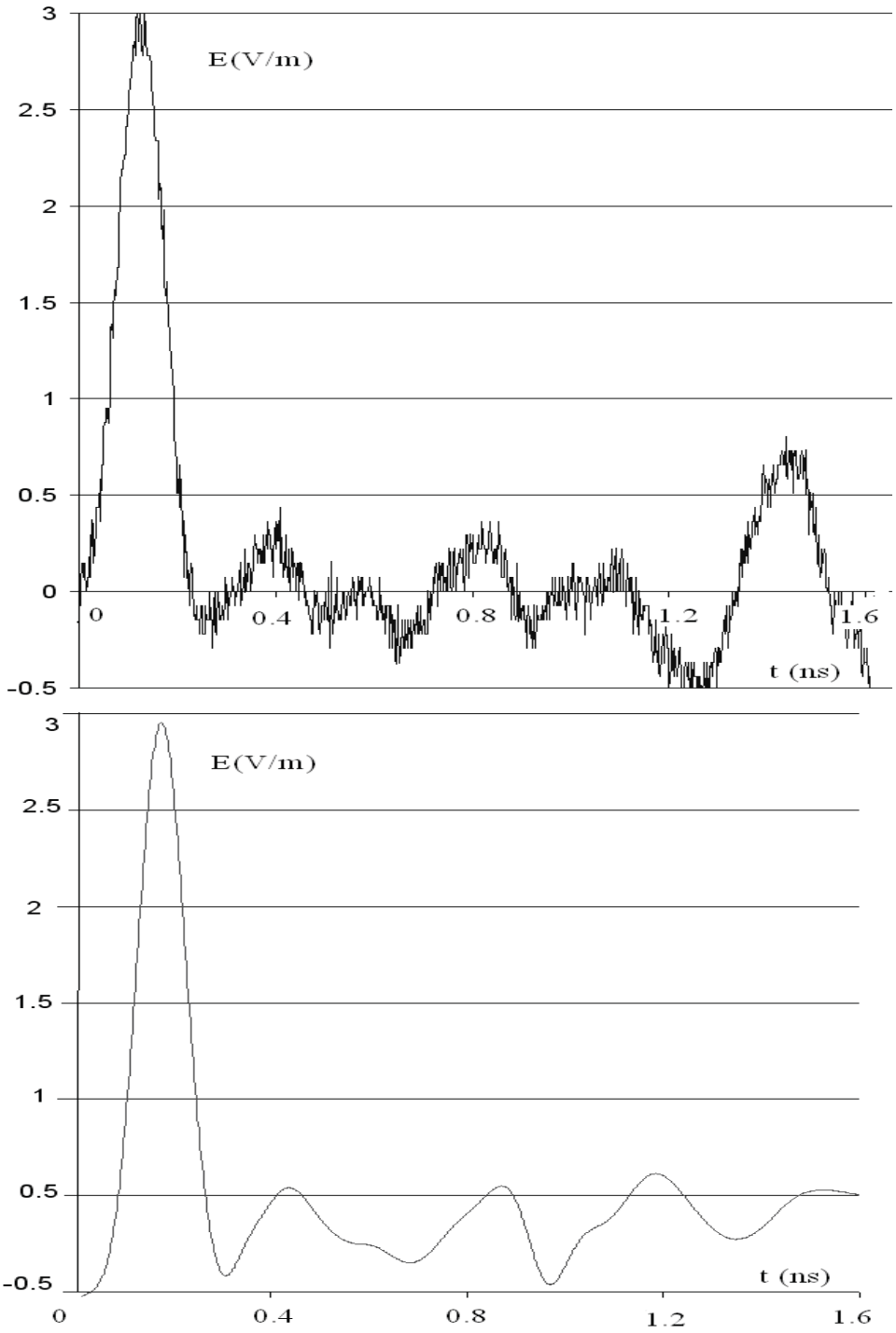

Figure 14: The derivative of the normalized prepulse term and the focal waveform from the B-Dot sensor.

In Figure 14 we compare the derivative of the normalized prepulse term and the focal waveform. They are oscillating at similar frequencies. This proves that the ripples in the prepulse cannot be associated with the feed arms near the reflector, by causality (speed of light). The ripples come from the prepulse not from the reflected waves; we do

not have any problem with the reflector and the feed arms. These ripples come either from the feed point or from the sensor. We considered the feed point first and measured the reflection coefficient (Γ) to check for problems with it.

One can see the reflection coefficient (Γ) values from Figure 15. It starts from -1 at short circuit, it goes to 0 when the current reaches the $50\ \Omega$ cable, it goes to 0.3 when it reaches the feed arms. Finally, it goes to -1 because the reflector feed arms are shorted. We can calculate the feed arms pulse impedance as

$$\Gamma = \frac{Z_L - Z_0}{Z_L + Z_0}. \tag{4.1}$$

$\Gamma = 0.3$ and $Z_L = 93\ \Omega$, which is close to the our analytical value of $Z_L = 100\ \Omega$ we do not have any problem in the feed arms geometry.

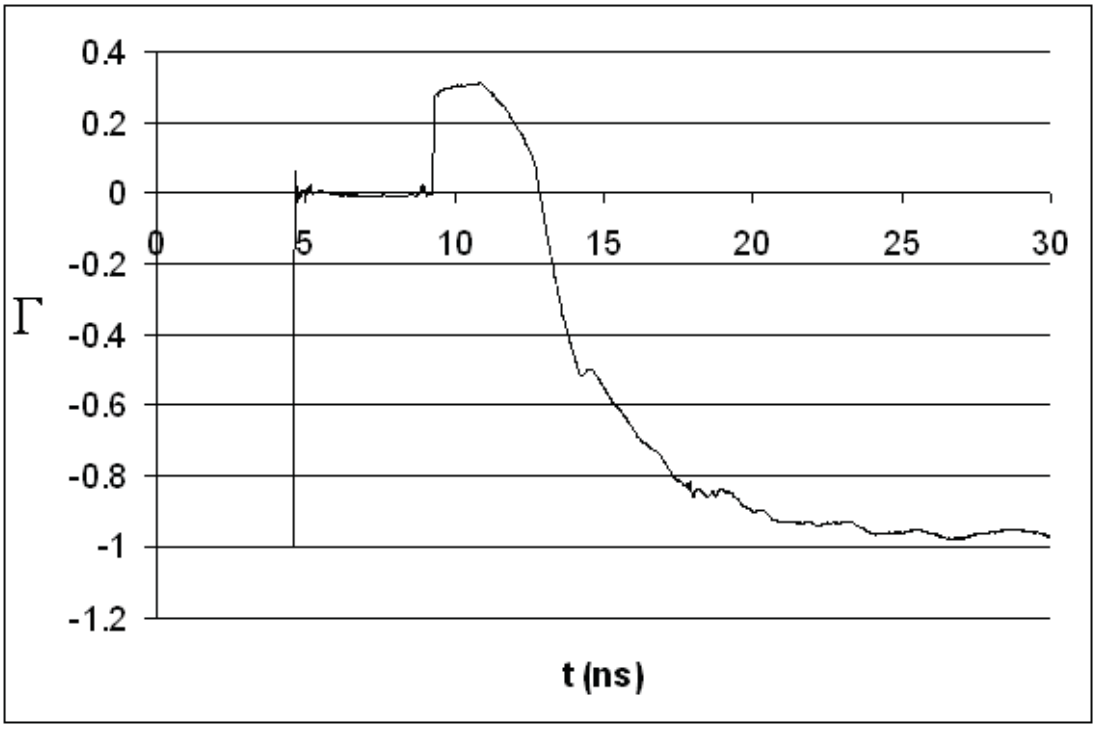

Figure 15: Reflection coefficient (Γ) measurements of the reflector with feed arms for impulse impedance calculation.

Figure 16 shows the ripples in the Γ with feed arm and open circuit case. If we compare the normalized derivative of the Γ with the focal waveform for feed arms and open circuit case as presented in Figure 17, they do not oscillate at the same frequencies, the transition between barrels may not cause these oscillations. Even if we have perfect connection between the feed arms and excitation point, it is difficult to obtain the actual focal waveform because of geometric restrictions. This can cause some differences but it should not be that significant.

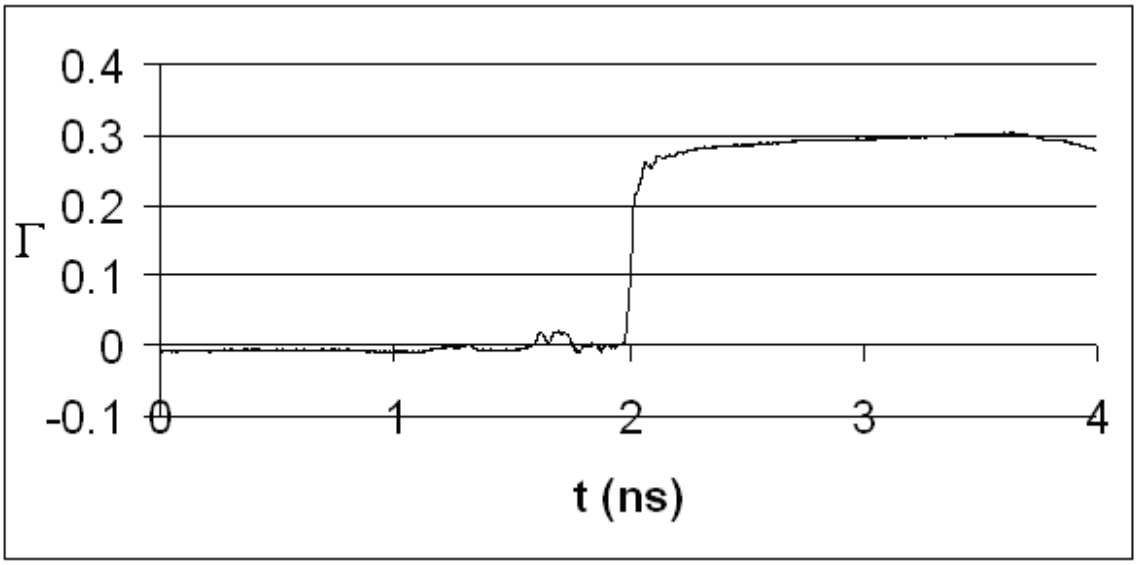

a)

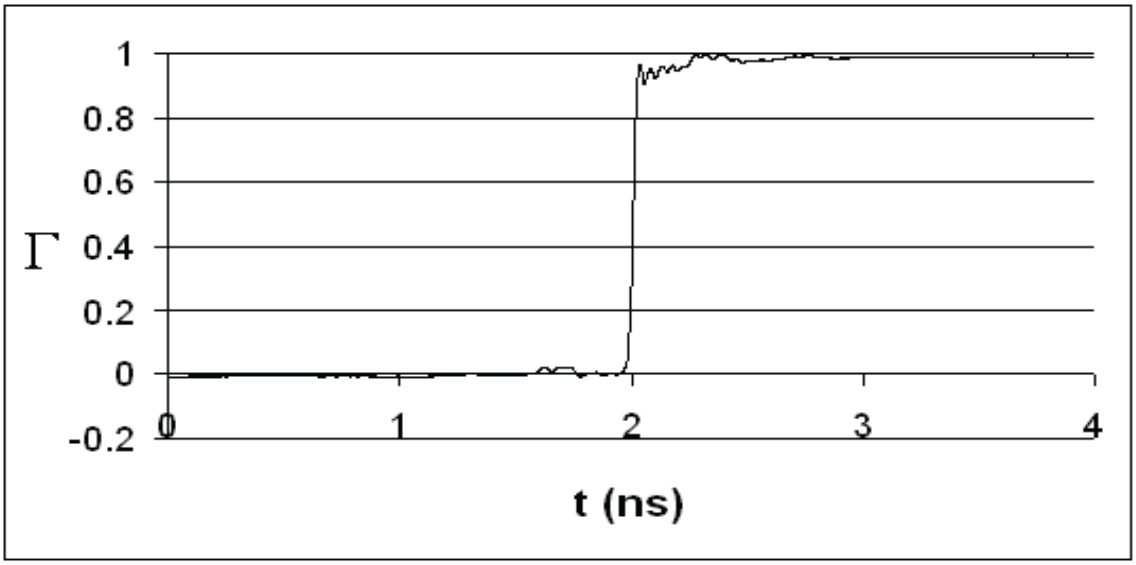

b)

Figure 16: Reflection coefficient (Γ) measurement a) with feed arms, b) open circuit.

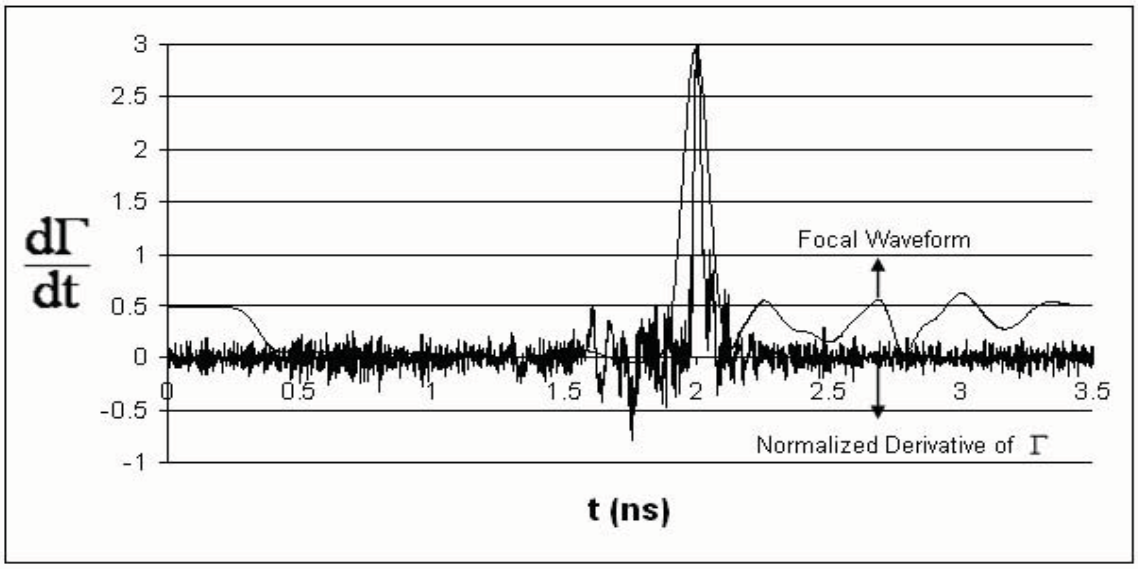

a)

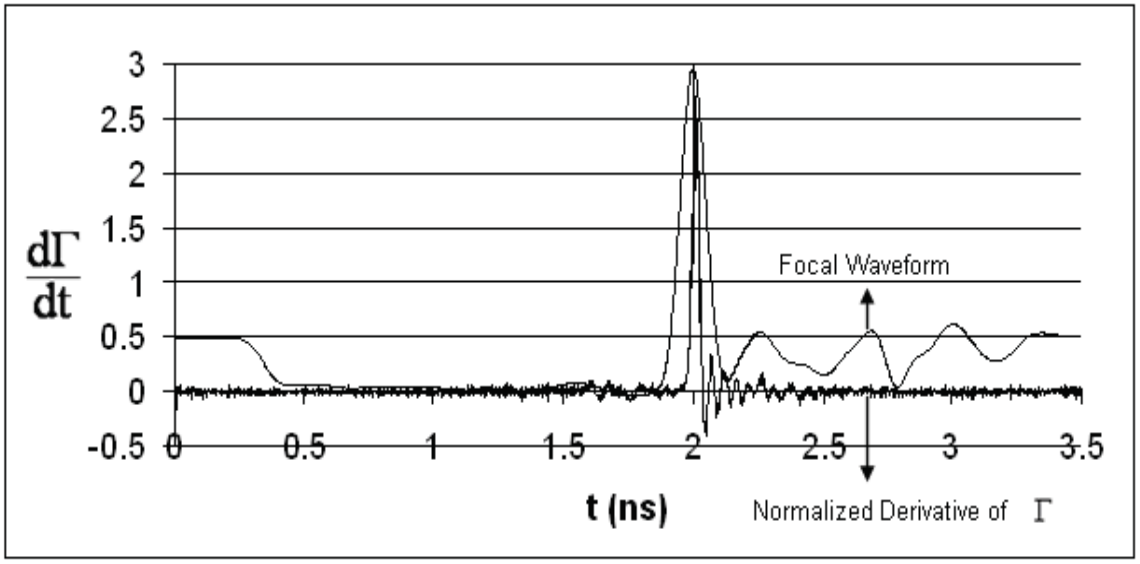

b)

Figure 17: Normalized derivative of Γ and focal waveform a) with feed arms b) open circuit.

We can see from Figure 12 that the B-Dot sensor causes the ringing in the postpulse. For the D-Dot probe we cannot obtain the expected analytical postpulse. There should also be another factor causing the ringing and the decrease in the amplitude. When the focal fields are calculated in [1], the aperture integral does not consider the feed arms and feed-arms' thicknesses. This can cause an error in the calculation of the impulse amplitude of the focal waveform; we believe this can cause the inconsistency between the analytical and experimental results. We want to see the effect of the feed arms on the aperture plane S_a, we performed another experiment. Assume we have an arbitrary piece

of metal (13cmX18cmX0.8cm) on the aperture plane S_a. Figure 18 shows the experiments that are presented in Figure 19.

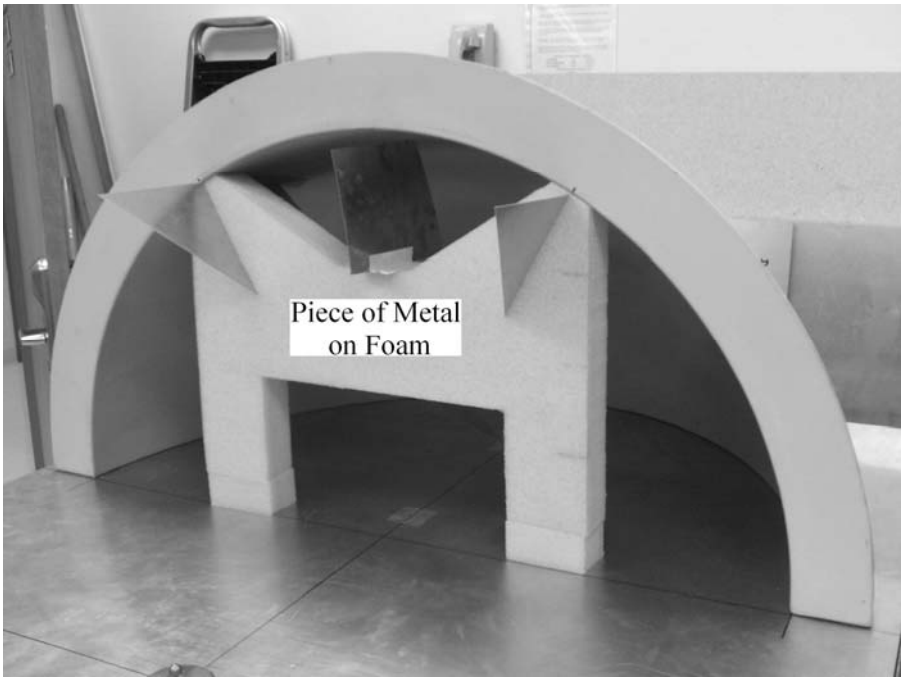

a)

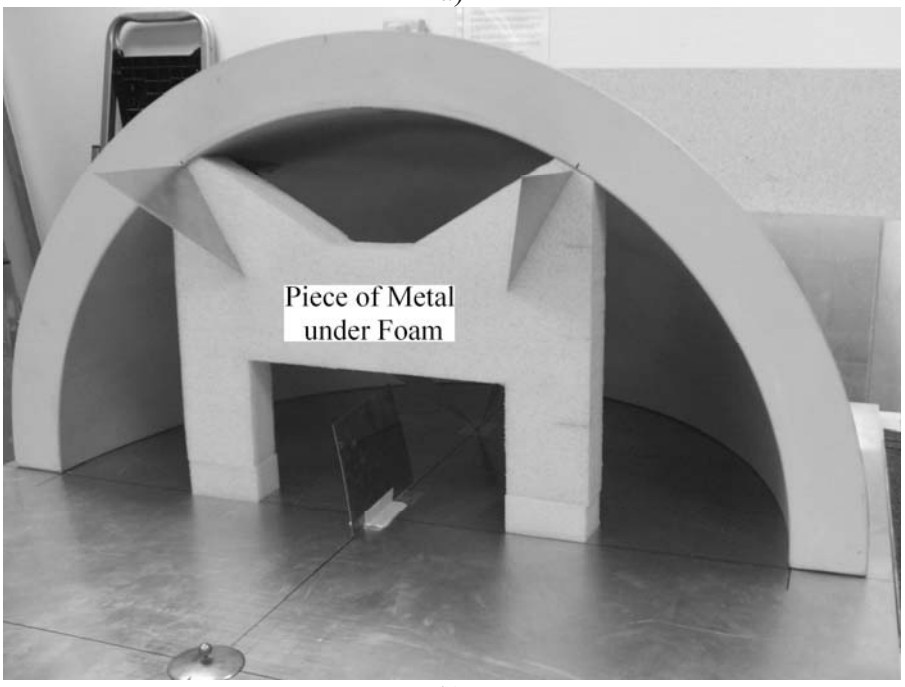

b)

Figure 18: 60^o four-feed arms a) with a piece of metal on the foam, b) with a piece of metal under the foam.

In Figure 18 metal conductors are on the aperture plane S_a where we integrate the fields to find the focal field at the second focal point. We try to see the effect of the feed arms on the aperture integral by inserting a piece of metal.

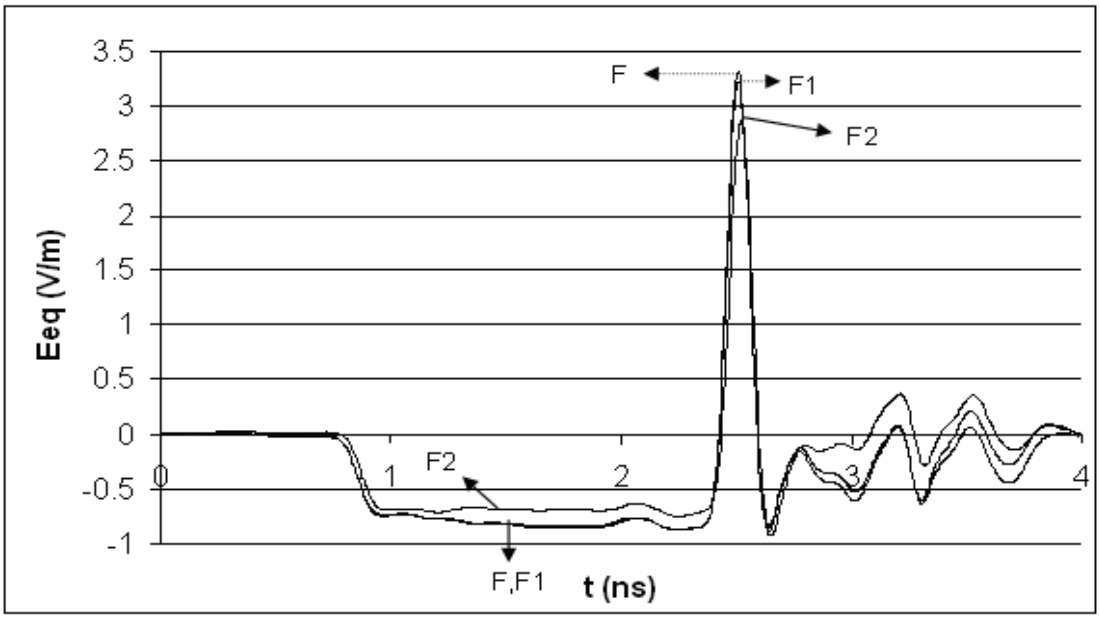

Figure 19: Focal waveforms from B-Dot probe for 60^o four-feed arms: F (focal waveform), F1 (focal waveform with a piece of metal on the foam), F2 (focal waveform with a piece of metal under the foam).

Table 3: Maximum values of F, F1 and F2.

Max(F (V/m))	Max(F1(V/m))	Max(F2(V/m))
3.32	3.23	2.86

Figure 19 presents the values of F (focal waveform), F1 (focal waveform with a piece of metal on the foam), and F2 (focal waveform with a piece of metal under the foam). The peak value of these waveforms are given in Table 3. In Figure 19, the behaviors of F and F1 are almost the identical. However, as seen from Table 3, F1<F but as expected this difference is not significant. This is because we have a null point right between the feed arms at the top of the reflector. We have a significant difference between the behavior of F and F2.

One can easily see that, although inserting a piece of metal on the top of the aperture plane S_a does not disturb the field that much because of the null point, inserting a piece of metal under the foam disturbs the focal field. If we insert a piece of metal under the foam, we have aperture scattering. Significant destructive interference occurs because of the feed arm itself and it blocks the reflected fields. The reflected fields are scattered through diffraction.

We can easily find the difference by comparing F and F2 from Table 3

$$Difference(\%) = \frac{F - F2}{F} * 100 = \frac{3.32 - 2.86}{3.32} * 100 = 14\%, \quad (4.2)$$

A 14% difference is a significant difference. If we compare F and F1, we have a difference of about 3%. The feed arm itself does not affect the prepulse because the prepulse is the direct radiated field from the feed arms we obtain almost the exact prepulse value in our experiments; however, any other metal scatters the prepulse field.

The geometric shape or alignment of the prolate-spheroidal reflector may also causes some errors. The misshape of the reflector will lead to a broader focus and smaller amplitude.

The prolate-spheroidal reflector was manufactured from fiber and the inside of the reflector is painted with copper conductive paint. The surface resistivity of the paint is <0.3 ohm/square at 1 mil dry film thickness; <0.10 ohm/square at 2 mil dry film thickness. We checked the reflection from the conductive paint on the reflector and measured about 99% reflection; however, there might be some hot spots that do not reflect very well and this can cause some errors.

We are consistent with Table 2 regarding the analysis of the differences. Focal waveforms from the slow D-Dot probe for 60^o four-feed arms: F, F1 and F2 are presented in Figure 20 and one can see the peak values for these focal waveforms in Table 4.

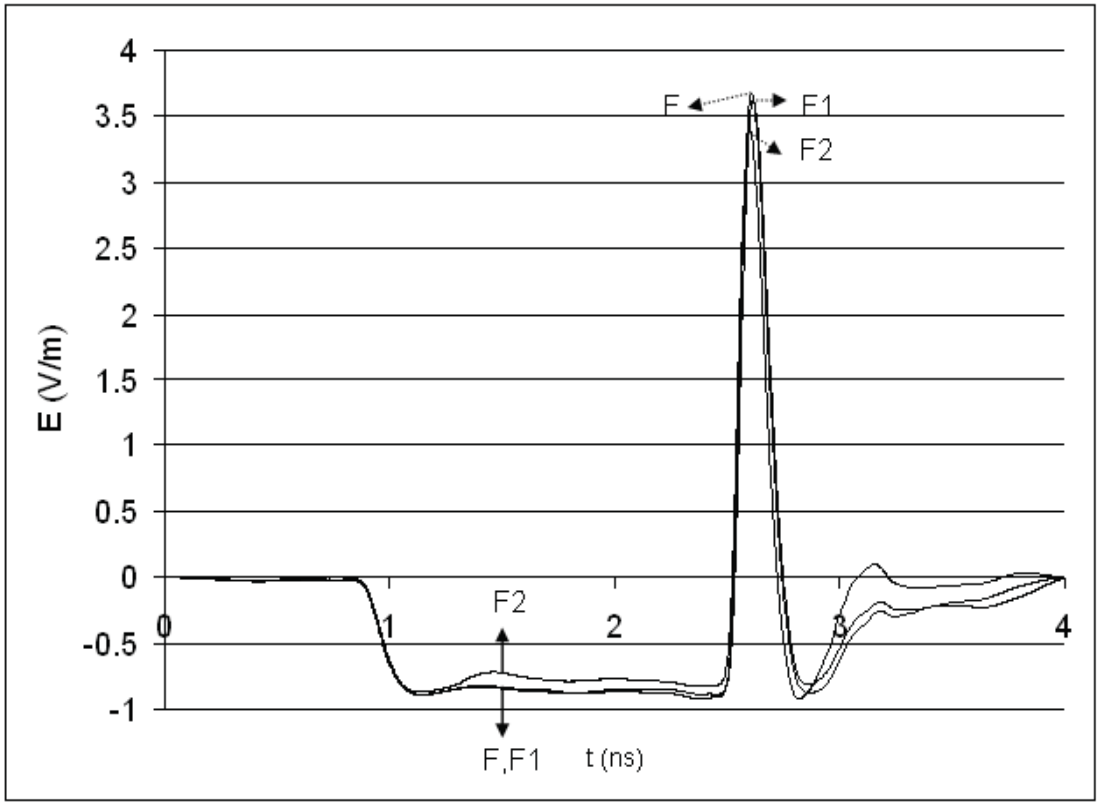

Figure 20: Focal waveforms from the slow D-Dot probe for 60^o four-feed arms: F (focal waveform), F1 (focal waveform with a piece of metal on the foam) , F2 (focal waveform with a piece of metal under the foam).

We can easily calculate the difference by comparing F and F2 from Table 4 and the resulting difference is 8%.

Table 4: Maximum values of F, F1 and F2.

Max(F (V/m))	Max(F1(V/m))	Max(F2(V/m))
3.67	3.62	3.40

We compare our analytical, numerical and experimental focal waveforms for a two-arm prolate-spheroidal IRA in Figure 21.

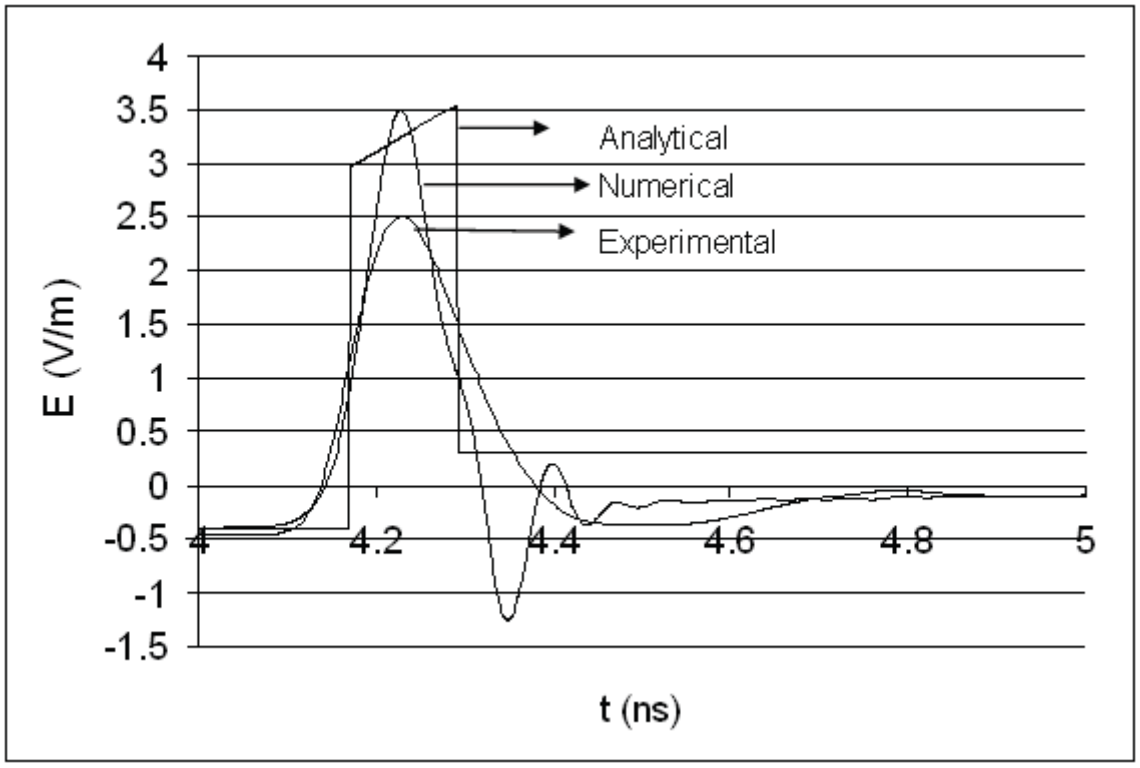

Figure 21: Analytical (slow D-Dot probe), numerical and experimental focal waveforms of a two-arm prolate-spheroidal IRA for tmr =119 ps.

One can see by comparing analytical, numerical and experimental focal waveforms that the prepulses agree very well. The analytical and numerical impulses' amplitudes agree as well. However, the experimental impulse amplitude is smaller than the others. It is also broader near the base. As discussed before, any misshape of the reflector may lead to this in the experiment. We have also a feed arm blockage effect that decreases the amplitude of the experimental impulse; however we did not see this effect in our numerical results. Our analytical result is based on an idealized assumption and it does not account for the feed arms. Finally, for all cases, the postpulse behaviors are different.

References

[1] C.E. Baum, "Focal waveform of a prolate-spheroidal impulse-radiating antenna (IRA)," Radio Science , accepted for publication.

[2] S. Altunc and C.E. Baum. "Extension of the analytic results for the focal waveform of a two-arm prolate-spheroidal impulse-radiating antenna (IRA)," Sensor and Simulation Note 518, Nov. 2006.

[3] K.H. Schoenbach, R. Nuccitelli and S.J. Beebe, "ZAP," IEEE Spectrum, Aug 2006, pp. 20-26.